Fabrication and surface plasmon coupling studies on the dielectric/Ag structure for transparent conducting electrode applications

Rina Pandey,[1,2] Basavaraj Angadi,[3] Seong Keun Kim,[2,4] Ji Won Choi,[2,4] Do Kyung Hwang,[1,2] and Won Kook Choi[1,2*]

[1]*Interface Control Research Center, Korea Institute of Science and Technology (KIST), Seongbuk Gu, Hwarangro 14 Gil 5, Seoul 136-791, South Korea*

[2]*Department of Nanomaterials Science and Engineering, Korea University of Science and Technology (KUST), Gajeong-ro 217, Yuseong-gu, Daejeon 305-350, South Korea*

[3]*Department of Physics, Bangalore University, Bangalore- 560 056, India*

[4]*Electronics Materials Research Center, Korea Institute of Science and Technology (KIST), Seongbuk Gu, Hwarangro 14 Gil 5, Seoul 136-791, South Korea*

[*]*wkchoi@kist.re.kr*

Abstract: The dielectric/Ag structures were fabricated on glass substrates using various metal oxides as dielectrics and their optical properties were studied through transmittance and ellipsometry measurements. The structures with 10 nm Ag film deposited on various metal oxides (Al_2O_3, ZrO_2, $SrTiO_3$, TiO_2, $CaCu_3Ti_4O_{12}$, WO_3 and HfO_2) of 30 nm showed enhancement in transmittance compared to bare Ag film in the visible region. This enhancement in transmittance was explained through suppression of surface plasmon coupling at the dielectric/Ag interface. The surface plasmon wave-vector (k_{SP}) was calculated using the measured dielectric constants for the dielectric and Ag through ellipsometry and employed to analyze the transmittance data. The k_{SP}/k_0 and δ_{SP} values were estimated and used to interpret the enhanced visible transmittance for different dielectric/Ag structures.

OCIS codes: (310.7005) Transparent conductive coatings; (240.6680) Surface plasmons; (260.2130) Ellipsometry and polarimetry; (310.1210) Antireflection coatings.

References and links

1. C. G. Granqvist, "Transparent conductors as solar energy materials: A panoramic review," Sol. Energy Mater. Sol. Cells **91**(17), 1529–1598 (2007).
2. C. G. Granqvist and A. Hultaker, "Transparent and conducting ITO films: new developments and applications," Thin Solid Films **411**(1), 1–5 (2002).
3. S. J. Kim and J. L. Lee, "Design of dielectric/metal/dielectric transparent electrodes for flexible electronics," J. Photon. Energy **2**(1), 021215 (2012).
4. L. Cattin, J. C. Bernede, and M. Morsli, "Toward indium-free optoelectronic devices: Dielectric/metal/dielectric alternative transparent conductive electrode in organic photovoltaic cells," Phys. Status Solidi A **210**(6), 1047–1061 (2013).
5. G. B. Murdoch, S. Hinds, E. H. Sargent, S. W. Tsang, L. Mordoukhovski, and Z. H. Lu, "Aluminum doped zinc oxide for organic photovoltaics," Appl. Phys. Lett. **94**(21), 213301 (2009).
6. A. Kumar and C. G. Zhou, "The Race to Replace Tin-Doped Indium Oxide: Which Material Will Win?" ACS Nano **4**(1), 11–14 (2010).
7. D. S. Ginley and C. Bright, "Transparent Conducting Oxides," MRS Bull. **25**(08), 15–18 (2000).
8. K. Ellmer, "Past achievements and future challenges in the development of optically transparent electrodes," Nat. Photonics **6**(12), 809–817 (2012).
9. J. L. Blackburn, T. M. Barnes, M. C. Beard, Y. H. Kim, R. C. Tenent, T. J. McDonald, B. To, T. J. Coutts, and M. J. Heben, "Transparent Conductive Single-Walled Carbon Nanotube Networks with Precisely Tunable Ratios of Semiconducting and Metallic Nanotubes," ACS Nano **2**(6), 1266–1274 (2008).
10. Y. M. Chang, L. Y. Wang, and W. F. Su, "Polymer solar cells with poly (3,4-ethylenedioxythiophene) as transparent anode," Org. Electron. **9**(6), 968–973 (2008).

#220324 - $15.00 USD Received 4 Aug 2014; revised 5 Sep 2014; accepted 5 Sep 2014; published 11 Sep 2014

11. S. De, T. M. Higgins, P. E. Lyons, E. M. Doherty, P. N. Nirmalraj, W. J. Blau, J. J. Boland, and J. N. Coleman, "Silver Nanowire Networks as Flexible, Transparent, Conducting Films: Extremely High DC to Optical Conductivity Ratios," ACS Nano **3**(7), 1767–1774 (2009).
12. J. Wu, H. A. Becerril, Z. Bao, Z. F. Liu, Y. S. Chen, and P. Penumans, "Organic solar cells with solution-processed graphene transparent electrodes," Appl. Phys. Lett. **92**(26), 263302 (2008).
13. H. Wu, L. B. Hu, M. W. Rowell, D. H. Kong, J. J. Cha, J. R. McDonough, J. Zhu, Y. Yang, M. D. McGehee, and Y. Cui, "Electrospun Metal nanofiber Webs as High-Performance Transparent Electrode," Nano Lett. **10**(10), 4242–4248 (2010).
14. L. B. Hu, H. S. Kim, J. Y. Lee, P. Peumans, and Y. Cui, "Scalable Coating and Properties of Transparent, Flexible, Silver Nanowire Electrodes," ACS Nano **4**(5), 2955–2963 (2010).
15. M. Chakaroun, B. Lucas, B. Ratier, C. Defranoux, J. P. Piel, and M. Aldissi, "High quality transparent conductive electrodes in organic photovoltaics devices," Thin Solid Films **518**(4), 1250–1253 (2009).
16. C. Guillén and J. Herrero, "Transparent conductive ITO/Ag/ITO multilayer electrodes deposited by sputtering at room temperature," Opt. Commun. **282**(4), 574–578 (2009).
17. Y. S. Jung, Y. W. Choi, H. C. Lee, and D. W. Lee, "Effects of thermal treatment on the electrical and optical properties of silver-based indium tin oxide/metal/indium tin oxide structures," Thin Solid Films **440**(1-2), 278–284 (2003).
18. D. R. Sahu, S. Y. Lin, and J. L. Huang, "ZnO/Ag/ZnO multilayer films for the application of a very low resistance transparent electrode," Appl. Surf. Sci. **252**(20), 7509–7514 (2006).
19. C. Guillén and J. Herrero, "TCO/metal/TCO structures for energy and flexible electronics," Thin Solid Films **520**(1), 1–17 (2011).
20. J. A. Jeong, Y. S. Park, and H. K. Kim, "Comparison of electrical, optical, structural, and interface properties of IZO-Ag-IZO and IZO-Au-IZO multilayer electrodes for organic photovoltaics," J. Appl. Phys. **107**(2), 023111 (2010).
21. J. M. Khoshman and M. E. Kordesch, "Optical Constants and band edge of amorphous zinc oxide thin films," Thin Solid Films **515**(18), 7393–7399 (2007).
22. P. B. Johnson and R. W. Christy, "Optical Constants of the Noble Metals," Phys. Rev. B **6**(12), 4370–4379 (1972).
23. W. L. David and W. R. Hunter, *Handbook of Optical Constants of Solids*, E.D. Palik, ed. (Academic, Orlando, Fla., 1985).
24. E. F. Schubert, "Refractive index and extinction coefficient of materials," (2004), http://homepages.rpi.edu/~schubert/Educational-resources/Materials-Refractive-index-and-extinction-coefficient.pdf
25. S. H. Choi, R. Pandey, C. H. Wie, Y. J. Lee, J. W. Lim, D. H. Park, S. J. Seok, Y. H. Jang, K. K. Kim, D. K. Hwang, D. J. Byun, W. K. Choi, "Highly transparent ZTO/Ag/ZTO multilayer electrode deposited by inline sputtering process for organic photovoltaic cells," Phys. Status Solidi A **1–8**, 1860–1867 (2014).
26. J. Tauc, *The Optical Properties of Solids* (North-Holland, Amsterdam, 1970).
27. H. Han, N. D. Theodore, and T. L. Alford, "Improved conductivity and mechanism of carrier transport in zinc oxide with embedded silver layer," J. Appl. Phys. **103**(1), 013708 (2008).
28. A. Indluru and T. L. Alford, "Effect of Ag thickness on electrical transport and optical properties of indium tin oxide-Ag-indium tin oxide multilayers," J. Appl. Phys. **105**(12), 123528 (2009).
29. G. D. Cody, T. Tiedje, B. Abeles, B. Brooks, and Y. Goldstein, "Disorder and the Optical-Absorption Edge of Hydrogenated Amorphous Silicon," Phys. Rev. Lett. **47**(20), 1480–1483 (1981).
30. J. R. Sambles, G. W. Bradbery, and F. Z. Yang, "Optical excitation of surface plasmons: an introduction," Contemp. Phys. **32**(3), 173–183 (1991).
31. W. L. Barnes, A. Dereux, and T. W. Ebbesen, "Surface Plasmon sub wavelength optics," Nature **424**(6950), 824–830 (2003).
32. K. Y. Hong and J. L. Lee, "Review Paper: recent Developments in Light Extraction Technologies of Organic Light Emitting Diodes," Electronics Materials Letters **7**(2), 77–91 (2011).
33. D. D. Li, D. H. Zhang, C. C. Yan, T. Li, Y. Wang, Z. G. Xu, J. Wang, and F. Qin, "Unidirectional surface Plasmon-polariton excitation by a compact slot partially filled with dielectric," Opt. Express **21**(5), 5949–5956 (2013).
34. H. Raether, *Surface Plasmon* ed. G. Hohler, ed. (Springer Berlin 1988).

1. Introduction

Transparent conducting oxides (TCO) are the integral part of the present day electro-optic devices as transparent conducting electrodes (TCE) in solar cells, displays and solid-state lighting [1, 2]. The two inherent properties, transmittance and the electrical conductivity of the TCOs are the important factors which make them the potential candidates for TCE applications [3, 4]. The present day display industry demands the compatibility of the fabricated devices on both rigid as well as flexible substrates for applications in wearable displays, rolled up mobile computers, flexible solar cells, etc [3]. This necessitates the

#220324 - $15.00 USD Received 4 Aug 2014; revised 5 Sep 2014; accepted 5 Sep 2014; published 11 Sep 2014

component TCEs should adapt to the flexibility without degrading their inherent properties. Indium tin oxide (ITO) has been the conventional TCO material used extensively in the fabrication of the electro-optic devices due to its high transmittance (>90%) and good electrical conductivity (R_s < 20 Ω/sq) [3, 4]. However, the exhaustive use of this material by the electro-optic industry, both at present and in near future, escalate its cost due to the limited resources of Indium (In). In addition, the ITO has some limitations, such as brittleness and high deposition temperature, which makes it incompatible for flexible and organic material based devices [4].

In the search for an alternate TCO, replacing ITO, some attempts were made to explore the suitability of Al doped ZnO (AZO), Ga doped ZnO (GZO) and F doped SnO_2 (FTO) due to their good transmittance and electrical conductivity as well as low material cost [5–8]. Attempts were also made utilizing carbon nano tubes [9], conducting polymers [10], metal-grid embedded in polymer [11], graphene [12], metal nano wires [13], semi-transparent metal electrodes and multilayered structures [14] as TCEs. However, the properties of all the above alternatives were not on par with those of ITO. Recently, the dielectric/metal/dielectric (DMD) structures, i.e. ITO/Ag/ITO are being explored as efficient TCEs [15–17]. The advantage of having metal sandwiched dielectric layers is achieving excellent electrical properties and with higher overall transmittance through suppressing the reflection from the metal layer in the visible region. Here again efforts were made to replace the ITO by other oxides, such as ZnO/Ag/ZnO [18], AZO/Ag/AZO [19], InZnO/Ag/InZnO [20], thereby minimizing the indium (In) usage and reducing the overall cost. These efforts resulted in the overall good electrical conductivity (R_s < 10 Ω/sq) and maximum transmittance of about 85%. However, there is no experimental study which gives the detailed analysis of the various dielectric/metal combinations on the overall transmittance of the structure and about the deciding factor in selecting a particular dielectric/metal combination and their various parameters such as the thickness, dielectric constant, optical properties etc.

In this work, in addition to addressing the above said parameters by designing and fabricating various dielectric/Ag structures, emphasis is given to the understanding of formation and suppression of Surface Plasmon coupling to enhance the overall transmittance of the structure. An exhaustive study with detailed experiments on various dielectric/Ag structures includes the studies on TCE properties correlating the observed transmittance with the band gap, dielectric constant, refractive index, extinction coefficient of the dielectrics and Ag. The structural, optical and electrical properties were studied for various dielectric/Ag structures with dielectrics having different dielectric constant values. The transmittance data was explained in terms of the surface plasmon effects by estimating the k_{SP}/k_0 and δ_{SP} values. The SP coupling showed a strong dependence on the k_{SP}/k_0 values. The observed enhancement in the visible transmittance in the dielectric/Ag structures is interpreted to the suppression of SP coupling, estimated from the ellipsometry data, due to the larger mismatch between k_{SP} and k_0 wave vectors.

2. Experimental

The dielectric/Ag thin films were deposited on glass substrates (Corning Eagle XG 0.7mm, Alkaline Earth Boro-Aluminosilicate). The single layer dielectric materials (Al_2O_3, $SrTiO_3$, TiO_2, $CaCu_3Ti_4O_{12}$, WO_3 and HfO_2) were deposited on glass substrates with optimized conditions. The TiO_2 was deposited by DC reactive sputtering, while WO_3 and $SrTiO_3$ were deposited using the RF sputtering at room temperature and the thickness of films was 30 nm. Films were fabricated at a constant power of 70 W for $SrTiO_3$ and 100 W for WO_3 with working pressure of 0.27 Pa and introducing mixed gas of pure Ar and forming gas (Ar and O_2) into the sputtering chamber while sputtering the $SrTiO_3$ and WO_3 target. Al_2O_3, HfO_2, and ZrO_2 were deposited by an atomic layer deposition (ALD) with optimized deposition conditions. The ZrO_2 oxides were deposited at 270°C and film thickness rate was 270 atomic layer deposition (ALD) cycles. The Al_2O_3 oxides were deposited at 110°C and film thickness

#220324 - $15.00 USD Received 4 Aug 2014; revised 5 Sep 2014; accepted 5 Sep 2014; published 11 Sep 2014

rate was 300 atomic layer deposition (ALD) cycles. The cycled periods includes TMA purging for 0.1 sec, N_2 purging for 15 sec and H_2O purging for 0.1 sec. Reactions were carried out in a customized flow type reactor with a nitrogen carrier gas at a flow rate of 200 sccm. Tetrakis (ethylmethylamino) zirconium as a zirconium precursor, Tetrakis (ethylmethylamino) hafnium as a hafnium precursor, and Trimethyl Aluminum (TMA) as an aluminum precursor were used for the deposition of ZrO_2, HfO_2, and Al_2O_3. The working pressure was 79 Pa for HfO_2, ZrO_2 and 29 Pa for AL_2O_3. $CaCu_3Ti_4O_{12}$ (CCTO) was prepared by Langmuir-Blodgett method and was deposited at room temperature at a constant power of 70 W and the working pressure was 0.27 Pa. The film deposition time was 18 min and the thickness of the film was 30 nm. The Ag films on different dielectric were deposited using radio frequency magnetron sputtering system with the working pressure of 0.27 Pa and RF power of 58 W. The target to substrate distance was fixed at 7 cm. For the uniformity of the films, the substrate was constantly rotated at a constant rate of 7 rpm during sputtering process.

X-ray diffraction (XRD) studies (Rigaku Dmax 2500/server) with CuK_α radiation (wavelength = 1.54 **Å**) was performed to investigate the crystallographic structure of bilayer thin films (dielectric/metal). The surface microstructure of dielectric and Ag films deposited on different dielectric substrate was measured using scanning electron microscopy (HR-LV NOVA- SEM, FEI). The optical transmittance of the films was measured using a UV-Visible spectrometer (Perkin Elmer UV/Vis spectrometer Lambda 18) in the wavelength range from 200~900 nm. The refractive index and extinction coefficient measurements were made using ellipsometry microscope (Ellipso Technology, Korea). The Essential MACLEOD: Optical Coating Design Software was used to simulate the dielectric/metal structure.

3. Results and discussion

3.1 Crystalline structural characterizations

The XRD patterns of the Ag, ZrO_2/Ag, $SrTiO_3$/Ag, TiO_2/Ag, $CaCu_3Ti_4O_{12}$/Ag, WO_3/Ag and HfO_2/Ag structures deposited on glass substrates are shown in Fig. 1(a). The metal oxide film thickness of 30 nm and Ag thickness of 10 nm were kept constant for all the structures. The XRD pattern of Ag film was compared with the standard Joint Committee on Powder Diffraction Standards (JCPDS) pattern and observed peaks indexed to (111), (200), (220) and (311) reflections. Most of the dielectric/Ag structures exhibit the peaks corresponding to the Ag layer on the amorphous background of the metal oxides, except for the case of ZrO_2/Ag, where, in addition to the peaks of Ag, there are (101), (103) and (211) peaks corresponding to polycrystalline ZrO_2. The metal oxide films deposited at room temperatures on glass substrates without any post deposition heat treatment. Hence all the structures reflect their amorphous nature except for ZrO_2. The polycrystalline nature of the ZrO_2 is due to the little high temperature (270°C) deposition through ALD process.

The sheet resistance of all the dielectric/Ag structures is listed in Table 1. These values vary from 6.34 Ω/sq to 8.15 Ω/sq, well below that of glass/Ag (8.6 Ω/sq) and in the acceptable limits for TCE applications. Figure 1 (b-e) shows the scanning electron microscope images of the Ag films on the glass substrate with different thicknesses exhibiting the surface microstructure. It is noteworthy that the surface morphology of the Ag films shows the Ag clusters for thickness of 7 nm and 8 nm and it clearly becomes smooth and continuous when the thickness exceeds 9 nm.

#220324 - $15.00 USD Received 4 Aug 2014; revised 5 Sep 2014; accepted 5 Sep 2014; published 11 Sep 2014

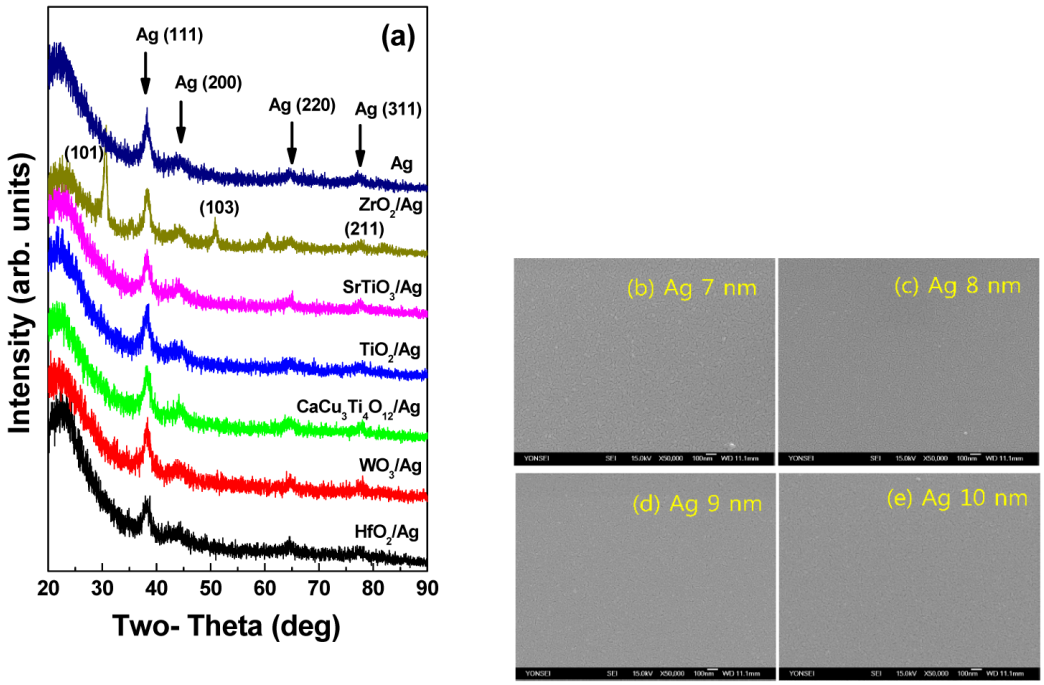

Fig. 1. (a) XRD plots of various dielectric/Ag structures grown on glass substrates and SEM images of Ag films deposited on glass with thickness (b) 7 nm, (c) 8 nm, (d) 9 nm and (e) 10 nm.

3.2 Optical properties

3.2.1 Optical constants from ellipsometry

Figure 2(a) and 2(b) shows the variation of refractive index (n) and extinction coefficient (k) with wavelength for various glass/dielectric structures obtained from ellipsometry measurements. The n and k exhibit a strong dispersion and decrease monotonically with increasing wavelength. These are good examples of physically reasonable spectra from the Cauchy–Urbach model for the optical constants of semiconductors with wide energy band gaps [21]. The average n values in the visible wavelength range for the various dielectric/Ag structures are shown in Table 1. The highest value being 2.547 for TiO_2 and lowest 1.637 for Al_2O_3. The k values are almost zero for all the dielectric/Ag structures in the visible range of wavelengths, indicating good transparency except a very small value in the range of 1.96 x 10^{-6} to 1.07 at below 430 nm for WO_3 and at all wavelengths for CCTO. It can also be seen from the figure that, the extinction coefficient shows a strong spectral dependence for $\lambda < 380$ nm (near band edge) for TiO_2, WO_3, CCTO and $SrTiO_3$, indicating that these structures becomes absorbent in the ultraviolet region. The observed n and k data for Ag (shown in Media 1 in the supplementary) and other oxides (shown in Fig. 2 and Media 1 in the supplementary) are similar to the data reported in literature [22–24].

#220324 - $15.00 USD Received 4 Aug 2014; revised 5 Sep 2014; accepted 5 Sep 2014; published 11 Sep 2014

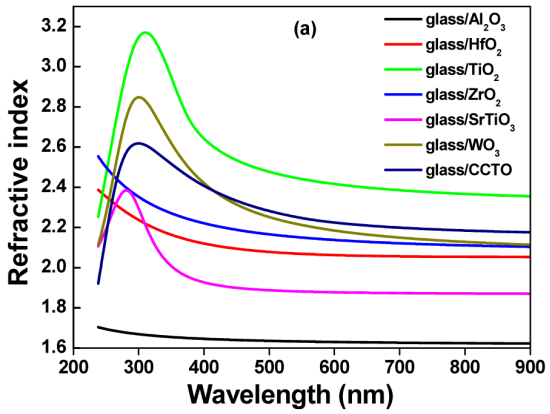

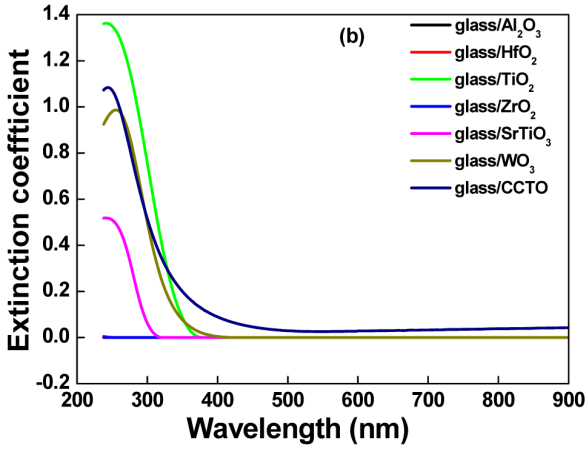

Fig. 2. (a) Refractive index (*n*) and (b) extinction coefficient (*k*) as a function of wavelength for various glass/dielectric substrates.

3.2.2 Transmittance of Dielectric (D) and Dielectric/Metal (D/M) structures

The optical transmittance spectra of the various metal oxides deposited on the glass substrate is shown in Fig. 3(a). With reference to the bare glass substrate, which show little more than 90% transmittance throughout the visible range of wavelengths (λ = 380-770 nm), the metal oxides show the varied transmittance in the visible region. The Al_2O_3 showing highest close to 90% transmittance, as much of that of glass substrate, the TiO_2 and $CaCu_3Ti_4O_{12}$ (CCTO) show the lowest about 70-75% and all the other oxides show the transmittance in the range of about 80-85%. The transmittance decreases at wavelength less than 400 nm in all the metal oxides due to the increased absorption in UV region corresponding to band to band transition. The varied nature of the transmittance in the metal oxide thin films (though most of their band gap energies are greater than 3 eV) might be due to the varied amount of absorption in the oxides, amorphous nature of the films as well as presence of some defects. Figure 3(b) shows the transmittance spectra of dielectric/Ag structures deposited on glass substrates with metal oxide thickness of 30 nm and Ag thickness of 10 nm. In our earlier work, we studied the effect of Ag thickness on the properties of the ZTO/Ag/ZTO DMD structures and found that the optimum thickness of Ag for the higher transmittance and lower sheet resistance was 9-10 nm [25]. The Ag thickness below 10 nm showed slightly higher sheet resistance due to the

#220324 - $15.00 USD Received 4 Aug 2014; revised 5 Sep 2014; accepted 5 Sep 2014; published 11 Sep 2014

discontinuous island structure of the Ag layer where as thickness above 10 nm showed decreased transmittance due to the increased absorption (opaqueness) of the Ag layer [25].

In Fig. 3(b), the transmittance of 10 nm Ag film, without metal oxide, is plotted as a reference. In general the transmittance increase with increase in wavelength reaches maximum value of 77.5% at around 367 nm and then decreases. The decrease in transmittance at longer wavelengths (towards the red part of the visible spectrum) is due to high reflectance from Ag. For bare Ag film, the transmittance decreases continuously at wavelength above 400 nm. This can be attributed to the increased absorption due to the surface plasmon coupling at the Ag/glass interface [3]. However, as compared to the bare Ag film, the transmittance of all the dielectric/Ag structures is enhanced in the entire visible range. This enhancement in transmittance in the visible wavelength is due to the suppression of the surface plasmons, which will be discussed in the next section (section 4.0). The optical band gap energies of dielectric/Ag structures were estimated by the following relationship [26],

$$\alpha h\nu = A\,(h\nu - E_g)^n \qquad (1)$$

where α is the absorption coefficient, $h\nu$ is the photon energy, A is a constant, E_g is the optical band gap, and n = 1/2 for direct transition.

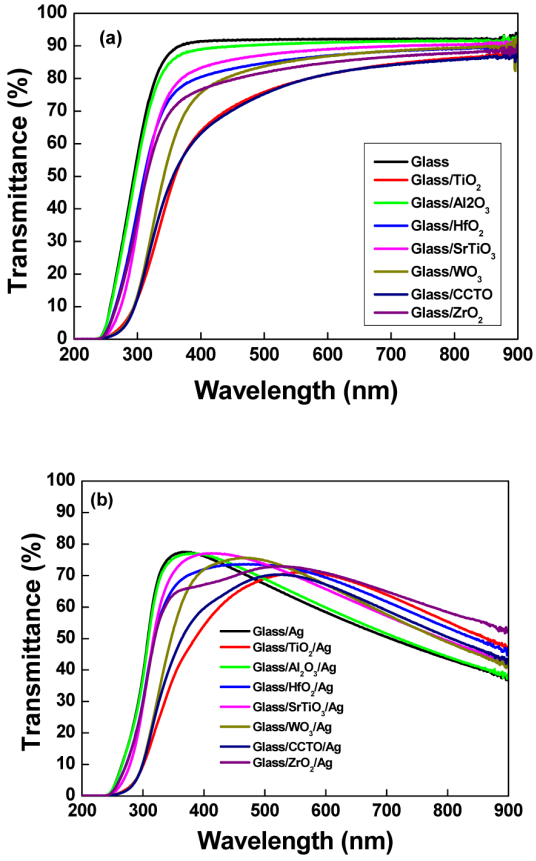

Fig. 3. Optical transmittance spectra for (a) glass/dielectric and (b) glass/dielectric/Ag structures.

#220324 - $15.00 USD Received 4 Aug 2014; revised 5 Sep 2014; accepted 5 Sep 2014; published 11 Sep 2014

Table 1. Electrical, optical and surface properties of dielectric/Ag structures

Sample	R_S (Ω/sq)	T_{ave} (%) (380-770 nm)	Band gap (eV)	n_{ave} (380-770 nm)	ε (550 nm)	$\left(\frac{k_{SP}}{k_0}\right)_{ave}$ (380-770 nm)
Ag	8.6	60.99	–	–	−10.61 + *i*0.54	–
Al_2O_3/Ag	6.34	62.21	4.65	1.637	2.66	1.49
$SrTiO_3$/Ag	6.79	66.78	4.37	1.91	3.57	1.70
HfO_2/Ag	6.8	68.22	4.54	2.095	4.28	1.82
ZrO_2/Ag	6.34	68.54	4.54	2.176	4.64	1.87
WO_3/Ag	6.34	66.77	3.92	2.31	4.88	1.96
CCTO/Ag	6.34	63.77	3.96	2.317	5.05	1.96
TiO_2/Ag	8.15	65.12	3.95	2.547	5.95	2.10

Figure 4 shows the typical $(\alpha hv)^2$ versus hv plots of dielectric/Ag structures. The optical band gap were estimated by the intercepts of the extrapolated linear regions of the curves to the energy axis (y = 0), assuming the direct band gap (n = 1/2) as all the curves are linear. The reduction in the band gap energies of the dielectric/Ag structures with respect to the reported values of the metal oxides may be due to the amorphous nature of the dielectric as well as the ionized Ag atoms in the Ag layer of the dielectric/Ag structures [27, 28]. The difference can be attributable to the fact that the structure of amorphous solid is characterized as an irregular arrangement of atoms. This disorder is known to influence the optical band "gap" of amorphous semiconductors as well [29, 21]. The average transmittance (T_{ave}) value in the wavelength range between 380~770 nm is shown in Table 1. The difference in the transmittance with the dielectric/Ag structure can be understood in terms of the surface plasmon (SP) contribution.

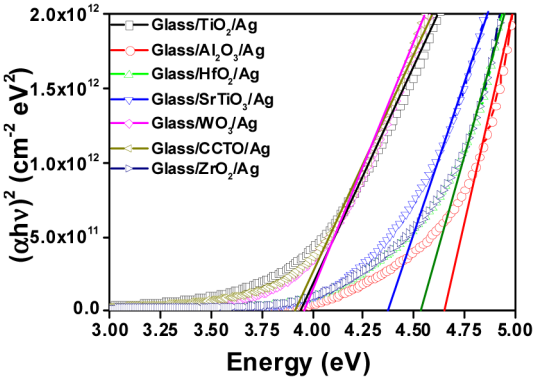

Fig. 4. Tauc's plots for various glass/dielectric/Ag structures.

4. Suppression of surface plasmon resonance

The SP coupling is a collective oscillation of electrons induced by the excitations of the conduction electrons in a metal produced at the interface of a metal and a dielectric. Solving the Maxwell's equation under the appropriate boundary conditions yields the SP dispersion relation [30, 31], i.e. the frequency-dependent SP wave-vector (k_{SP}),

$$k_{SP} = k_0 \sqrt{\frac{\varepsilon_d \varepsilon_m}{\varepsilon_d + \varepsilon_m}} \tag{2}$$

where ($k_0 = \omega/c$) is the wave-vector of a photon, ε_d and ε_m are the frequency dependent dielectric permittivity of the dielectric and metal (Ag), respectively. The SP coupling is

#220324 - $15.00 USD Received 4 Aug 2014; revised 5 Sep 2014; accepted 5 Sep 2014; published 11 Sep 2014

induced at the dielectric/Ag interface when the real part of the dielectric constant of metal is negative and its magnitude is greater than that of dielectric. In addition, the planar SP coupling is non-radiative as $k_{SP} > k_0$ in free space at the same frequency. Thus, we can increase the optical transmittance of Ag by selecting suitable dielectric material with ε_d greater than ε_{Ag}. To explain the observed transmittance of our various dielectric/Ag structures, we calculated the ε_d and ε_{Ag} values using the experimentally measured refractive index (n) and extinction coefficient (k) from ellipsometry,

$$\varepsilon' = n^2 - k^2 \tag{3}$$

$$\varepsilon'' = 2nk \tag{4}$$

Where ε' and ε'' are the real and imaginary part of permittivity, respectively. The ε' and ε'' values obtained for various dielectric materials are plotted in Fig. 5. The ε_d (ε' = for visible wavelengths) values at 550 nm (visible range) are tabulated in Table 1 for all the dielectric along with that of Ag. The ε_d values obtained for all the dielectrics are much lesser compared to the reported values, mainly due to the amorphous nature of our samples as they are deposited at room temperature. From the table it can be seen that all the dielectric materials have the ε_d values smaller than that of Ag (even if we consider the value of 9.7 reported for Ag) [32]. The Al_2O_3/Ag structure with ε_d = 2.68 the lowest value, has larger contribution to the SP coupling and there by showing greater absorption or lowest transmittance (Fig. 3(b)) in the visible region. The TiO_2/Ag structure with highest ε_d = 6.52 has least SP coupling and hence the highest transmittance in the visible region. The k_{SP}/k_0 ratio can be used as an estimate for SP coupling, where k_{SP} is a wave vector required to excite the surface plasmons at the dielectric/Ag interface [33].

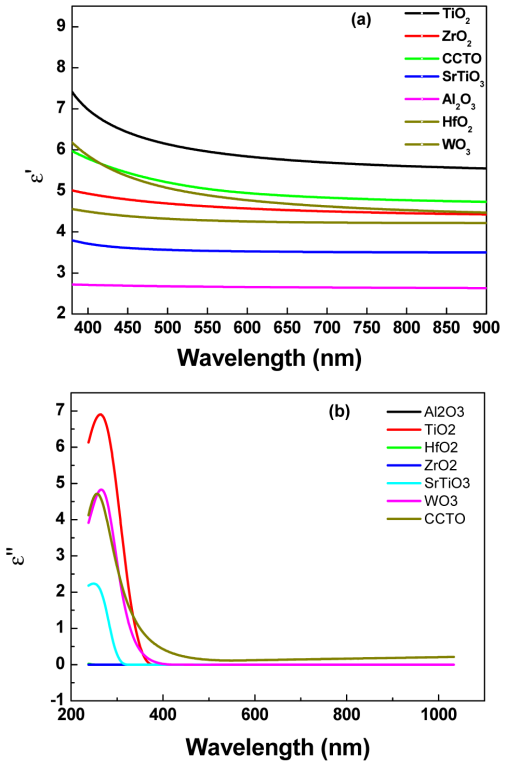

Fig. 5. (a) Real (ε') and (b) imaginary (ε'') part of permittivity as a function of wavelength for various glass/dielectric structures.

#220324 - $15.00 USD Received 4 Aug 2014; revised 5 Sep 2014; accepted 5 Sep 2014; published 11 Sep 2014

Figure 6 shows the plot of k_{SP}/k_0 as a function of wavelength. This data supports the above analysis. From the fig. it is clear that the SP coupling is wavelength dependent. Higher wave-vector components are required to excite the surface plasmons as the wavelength increases in the visible range. However, the decrease in k_{SP}/k_0 at lower wavelengths ($\lambda < 350$ nm) indicates an increased contribution from the SP coupling due to the air/Ag interface. In this case, SP excited at air/Ag interface will be much stronger than the dielectric/Ag interface. Now, if we compare the various dielectric/Ag interfaces, SP coupling depends on the extent of mismatch of the wave vectors k_{SP} and k_0 for different combinations of dielectric and Ag. Table 1 show the calculated average values of k_{SP}/k_0 for the visible region using the average values of ε_d and ε_{Ag}. The Al_2O_3/Ag showed the least mismatch with average ratio of $k_{SP}/k_0 = 1.49$ show stronger SP coupling as it can excite the surface plasmons to a larger extent. The average ratio k_{SP}/k_0 increases as we can see from the Table 1 and TiO_2/Ag showed the large mismatch with average ratio of $k_{SP}/k_0 = 2.10$ indicating relatively weaker SP coupling. This analysis perfectly corroborating with our observed enhancement in the optical transmittance data presented in Fig. 3(b).

The higher enhancement in the visible transmittance for the TiO_2/Ag structure can be correlated to the suppression of the SP coupling due to the larger mismatch between k_{SP} and k_0 wave vectors. Similarly, the lowest enhancement in the visible transmittance for the Al_2O_3/Ag structure can be correlated to presence of SP coupling due to the lowest mismatch between k_{SP} and k_0 wave vectors. The other dielectric/Ag structures exhibit the intermediate enhancement due to the relatively increased suppression of SP coupling. The calculated transmission spectra, shown in Fig. 7, for the dielectric/Ag structures using the Essential MACLEOD: Optical Coating Design Software clearly corroborates the above interpretation.

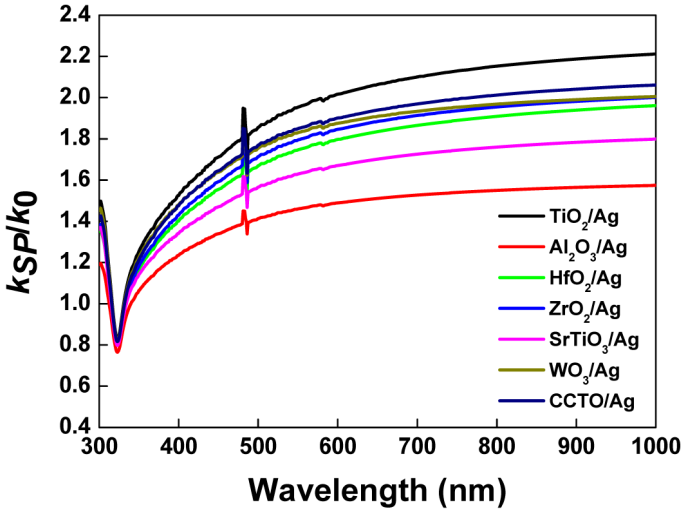

Fig. 6. Variations of K_{SP}/K_o as a function of wavelength for various dielectric/Ag structures.

#220324 - $15.00 USD Received 4 Aug 2014; revised 5 Sep 2014; accepted 5 Sep 2014; published 11 Sep 2014

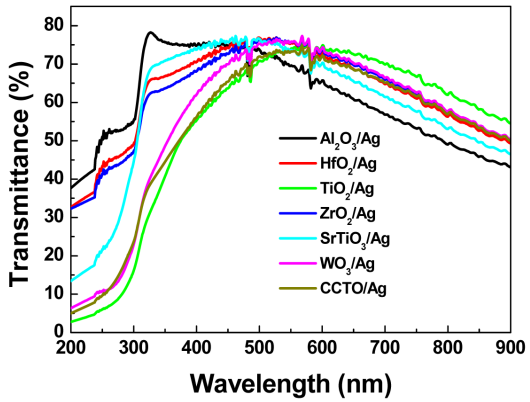

Fig. 7. Calculated ttransmittance spectra for various dielectric/Ag structures.

Since, we have SP coupling in all our dielectric/Ag structures; it is interesting to understand the propagation of surface plasmons. Once the light has been converted to SP mode, it will propagate on the Ag surface but will gradually attenuate owing to losses arising from absorption in Ag. This attenuation depends on the ε_{Ag} at the oscillation frequency of SP. The propagation length (δ_{SP}) can be found seeking the imaginary part (k''_{sp}) of the complex SP wave vector, $k_{sp} = k'_{sp} + ik''_{sp}$, from the SP dispersion Eq. (2) [31–34],

$$\delta_{SP} = \frac{1}{2k''_{SP}} = \frac{c}{\omega}\left(\frac{\varepsilon'_m + \epsilon_d}{\varepsilon'_m \epsilon_d}\right)^{\frac{3}{2}} \frac{\left(\varepsilon'_m\right)^2}{\epsilon''_m} \tag{5}$$

where ε'_m and ϵ''_m are the real and imaginary parts of the dielectric function of the metal, that is. $\epsilon_m = \varepsilon'_m + i\epsilon''_m$. We calculated the δ_{SP} for various dielectric/Ag structures and the data is plotted in Fig. 8. It can be seen from the Fig. that the δ_{SP} values are high for the Al_2O_3/Ag structures and the values are in the range of 2 – 12 μm for the visible range. The δ_{SP} decreases for the structures with increase in ε_d of dielectric, it has lowest value for the TiO_2/Ag structure with around 2 - 4 μm for which ε_d = 6.52. The δ_{SP} is strongly depending on the ε_d values of the dielectric. This indicates that even if we have SP modes active in these dielectric/Ag structures, they are active within this short distance and then die off. By properly selecting a dielectric with ε_d values higher than the ε_{Ag}, the k_{SP} and δ_{SP} can be minimized and hence the transmittance of the dielectric/Ag structure can be enhanced.

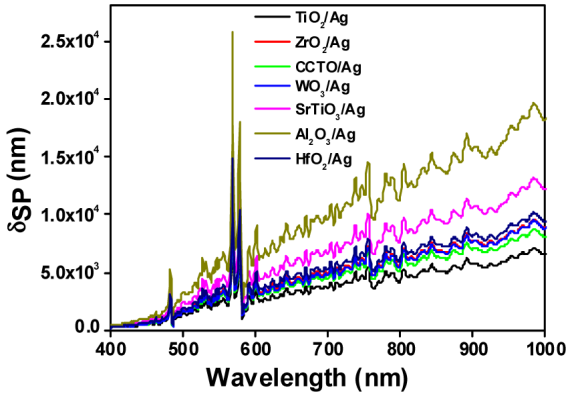

Fig. 8. Variations of δ_{SP} as a function of wavelength for various dielectric/Ag structures.

#220324 - $15.00 USD Received 4 Aug 2014; revised 5 Sep 2014; accepted 5 Sep 2014; published 11 Sep 2014

5. Conclusions

The dielectric/Ag structures with various metal oxides such as Al_2O_3, ZrO_2, $SrTiO_3$, TiO_2, $CaCu_3Ti_4O_{12}$, WO_3 and HfO_2 as dielectric layer were fabricated with optimized thickness of dielectric and Ag. The structural, optical (transmittance, refractive index, extinction coefficient, optical band gap) and electrical (sheet resistance) properties were studied for various dielectric/Ag structures. The transmittance data was explained in terms of the surface plasmon effects by estimating the k_{SP}/k_0 and δ_{SP} values. The SP coupling showed a strong dependence on the k_{SP}/k_0 values. The enhanced visible transmittance in the dielectric/Ag structures was due to the suppression of SP coupling due to the larger mismatch between k_{SP} and k_0 wave vectors.

Acknowledgments

This work was partially supported by the Converging Research Centre Program through the Ministry of Science, ICT and Future Planning, Korea (2013K000199) and Industrial Core Technology Development program (2MR2010) and ATC program (10048659) from Ministry of Trade, Industry (MOTIE), Republic of Korea.

#220324 - $15.00 USD Received 4 Aug 2014; revised 5 Sep 2014; accepted 5 Sep 2014; published 11 Sep 2014